

Enhancement of finite wavevector nematic fluctuations in the superconducting state of $\text{Ba}(\text{Fe}_{1-x}\text{Co}_x)_2\text{As}_2$

F. Weber¹, D. Parshall^{2,3}, L. Pintschovius¹, J.-P. Castellan^{1,4}, M. Merz¹, Th. Wolf¹, and D. Reznik³

¹ Institute for Solid State Physics, Karlsruhe Institute of Technology, 76021 Karlsruhe, Germany

² NIST Center for Neutron Research, National Institute of Standards and Technology, Gaithersburg, Maryland 20899, USA

³ Department of Physics, University of Colorado at Boulder, Boulder, Colorado, 80309, USA

⁴ Laboratoire Léon Brillouin (CEA-CNRS), CEA-Saclay, F-91191 Gif-sur-Yvette, France

Abstract

Nematic order is ubiquitous in liquid crystals and is characterized by a preferred direction in an otherwise isotropic liquid. Recently a similar symmetry breaking has been observed in some electronic phases in quantum materials related to high temperature superconductors. We investigated the prototypical Fe-based high-temperature superconductor $\text{Ba}(\text{Fe}_{1-x}\text{Co}_x)_2\text{As}_2$ where the interplay of electronic nematic order and superconductivity is well established. Previous measurements found a strong suppression of nematic fluctuations at zero momentum in the superconducting state, but what happens at nonzero momentum is unknown. We found that fluctuations at small momenta, which correspond to wavelengths of as much as 25 unit cells, do not compete with superconductivity. Instead they continue to grow below superconducting T_c . This result contrasts the conventional picture where the behavior at the ordering wavevector ($q=0$) and nearby (small) wavevectors should be similar. Our results imply the existence of a length scale larger than 25 unit cells that is important for understanding of the interplay between nematicity and superconductivity.

Introduction

In some quantum materials the high temperature crystal structure has a tetragonal (fourfold) symmetry, but the electrons self-organize into a state with orthorhombic (twofold) symmetry below a certain temperature [1]. Due to the analogy with nematic liquid crystals, such electronic phases are called nematic [2]. In copper oxide superconductors they may be associated with the formation of charge stripes whose role is not yet clearly established [3-6]. In Fe-based superconductors electrons can fluctuate between nearly nested sheets of the Fermi surface preferentially along one of two orthogonal directions. This lowering of the symmetry from fourfold to twofold would lead to orbital ordering and the orthorhombic atomic lattice distortion. Alternatively, this symmetry lowering can occur due to orbital ordering [7-9]. Either way, this phase is nematic as long as long-range magnetic order does not form. The existence of such nematic orbitally-ordered phase is well supported in at least one family of materials, $\text{Ba}(\text{Fe}_{1-x}\text{Co}_x)_2\text{As}_2$ [10].

Without magnetoelastic coupling the atomic lattice would be tetragonal [11]. The coupling to the anisotropic magnetic fluctuations shortens bond lengths along one direction and lengthens them along the other [12-16]. It has been shown that this orthorhombicity of the atomic lattice reflects electronic nematic order [17]. Thus, the nematic order parameter has zero wavevector ($q = 0$) and is proportional to the deviation from tetragonal symmetry.

Nematic fluctuations associated with the second order structural phase transition to the nematic phase [for a review see Ref. [18]] have been extensively investigated at $q = 0$ [19-21], but little

is known about their q -dependence. We investigated $q > 0$ nematic fluctuations by detailed inelastic neutron scattering measurements of phonons that couple to them. Our results show that these fluctuations intensify on cooling in the tetragonal phase but are suppressed by the nematic (structural) transition and by formation of short-range orthorhombic distortions. On entering the superconducting state fluctuations continue the buildup that begins at much higher temperatures. In other words, in contrast to $q = 0$ fluctuations, the fluctuations at $|q| = 0$ do not compete with superconductivity.

Results

$q = 0$ nematic fluctuations soften the shear mode C_{66} previously measured by resonant ultrasound [21] and 3-point bending techniques [19]. Transverse acoustic phonons dispersing in the [010] direction, which connect to this shear mode in the long wavelength limit, soften on approach to the phase transition temperature in BaFe_2As_2 and SrFe_2As_2 [22]. Close correlation with magnetic properties [23] and the similarity of the softening with the temperature-dependence of C_{66} provided strong evidence that these phonons couple to nematic fluctuations with the same wavevector. Following the experimental procedure of Reference [23] we first investigated underdoped samples where magnetic and structural phase transitions occur at different temperatures, T_N and T_S , respectively [10]. Then we extended this work to optimally doped and overdoped compositions. Since doped samples are superconducting, we also measured the temperature-dependence of the same phonons across the superconducting transition temperature, T_c .

Figure 1 illustrates how the softening of long-wavelength acoustic phonons appears in the raw data. We performed constant energy scans along $(2, h, 0)$, $-0.1 \leq h \leq 0.1$. Two peaks on opposite sides of $h = 0$ correspond to acoustic phonons propagating along h and along $-h$. Tilted resolution ellipsoid can result in an asymmetric lineshape with a broad peak on the defocusing side and a narrow one on the focusing side, e.g. in the optimally doped sample (Fig. 1b). In our measurements of the under- and optimally doped samples, the resolution function picked up a small contribution from more steeply dispersing longitudinal acoustic phonons centered at $h = 0$ because of imperfect resolution in Q . Hence, our constant energy scans were fit with three peaks with the middle peak position fixed to $h = 0$. When the phonons soften, the scan crosses the dispersion curves at larger $|h|$ and the separation between the peaks increases. This is very clear from comparison of the room temperature data and lower temperatures (Fig. 1). Effects are more subtle but still visible on cooling through T_c .

We measured the detailed temperature dependence of these effects (Fig. 2). In the underdoped samples the phonon first softens on cooling from room temperature (Fig. 2a,b) but then hardens below T_S where it follows the orthorhombic order parameter (short-dashed [red] line in Fig. 2b determined in a high-resolution diffraction configuration on the 1T TAS) until superconductivity sets in at T_c . A similar reversal was reported for undoped samples where T_S and T_N are essentially the same. In the under-doped samples where the two transitions are well separated ($\Delta T \approx 10$ K), there is no effect at T_N . Superconductivity suppresses the orthorhombic order parameter, which, by itself, should soften the phonons. However, the observed phonon softening is larger than the orthorhombic order parameter decrease indicating that nematic fluctuations intensify faster than expected from a simple suppression of orthorhombicity by superconductivity.

In the optimally-doped sample, the phonons soften from 300 K to about 70 K (Figs. 2c,d). In this temperature range the softening is close to linear at $h \approx 0.09$, but at $h \approx 0.06$ it accelerates at lower temperatures and resembles the reported softening of C_{66} (solid blue line in Fig. 2c) [19]. Then the temperature dependence is nearly flat down to T_c where the softening resumes and continues down to base temperature. In the overdoped sample ($x = 9.5$ %) the initial hardening for $E = 1.5$ meV on cooling from room temperature reflects the increased separation [within the (T, x) phase diagram] from the orthorhombic phase and is consistent with C_{66} results

for similarly doped samples (solid line in Fig. 2e) [19]. Below $T = 150$ K, the softening induced by nematic fluctuations takes over. Then, the temperature dependence is similar to that observed at optimal doping, except there is a clear softening at all temperatures. The softening near $h = 0.055$ continues below T_c with only a small temperature region, $T_c = 17 \text{ K} \leq T \leq 35 \text{ K}$ exhibiting a slightly reduced softening.

How can we understand this behavior? First, it is instructive to compare the $q > 0$ nematic fluctuations to the $q = 0$ fluctuations reflected in the shear modulus C_{66} . Intensifying nematic fluctuations at $q = 0$ soften C_{66} on cooling towards the phase transition as measured by resonant ultrasound [21] and three-point bending experiments [19]. In fact, three-point bending experiments measure the Young's modulus $Y_{[110]}$. However, the temperature dependence of $Y_{[110]}$ in $\text{Ba}(\text{Fe}_{1-x}\text{Co}_x)_2\text{As}_2$ is dominated by that of the C_{66} shear modulus as demonstrated in Ref. [19]. The softening reverses on cooling below the superconducting transition at optimal doping and beyond [19,21], i.e. nematic fluctuations at $q = 0$ compete with superconductivity [24-27].

Strain-stress measurements showed that these nematic fluctuations display quantum critical behavior associated with the quantum (zero temperature) phase transition from the orthorhombic to tetragonal ground state induced by Co doping [20].

C_{66} data indicated by the blue solid lines in Fig. 2 are unreliable in the orthorhombic phase due to twinning, so a comparison with phonons in the underdoped samples is impossible below T_S . In these samples the phonon softening from 300 K to T_S at nonzero q is much smaller than at $q = 0$ (see Fig. 2a). This result is consistent with the strongest nematic fluctuations appearing at the nematic ordering wavevector $q = 0$ in agreement with conventional theory. In the optimally-doped sample which does not become orthorhombic, the softening from 300 K to T_c at $h = 0$ (blue line) and $h = 0.05$ (data points) is roughly the same. In the overdoped sample nematic fluctuations intensify at low temperatures on increasing h . This doping-dependence indicates that nematic fluctuations spread out in q -space with increased doping, with a maximum moving away from $q = 0$ in overdoped samples. This behavior is qualitatively consistent with reduced Fermi surface nesting at $q = 0$, but more theoretical and experimental work is necessary.

We now discuss the low temperature behavior of optimally-doped and overdoped samples, which are always tetragonal and, therefore, never twinned.

The TA mode wavevector in the optimally-doped sample at $E = 1$ meV (Fig. 3a) is temperature-independent between 70 K and $T_c = 25$ K. A similar feature is absent in the C_{66} data (blue line in Fig. 3a) but is also seen further away from the zone center, i.e. at higher phonon energies (Figs. 2c,d). Here, we argue that this flat region originates from orthorhombic microdomain formation due to proximity to the orthorhombic phase. Figure 3b shows that the intensity of the (2,0,0) neutron diffraction Bragg peak increases slowly below room temperature and then sharply rises below 70 K until the reversal at T_c in the optimally-doped sample. Whereas an increase of Bragg scattering on cooling is expected due to reduced thermal motion of the atoms, i.e. due to a temperature dependent Debye-Waller factor, the sudden rise below $T = 70$ K is unusual. We relate it to mosaic effects: During Bragg scattering all neutrons that come in at the angle that matches the Bragg condition are scattered. If the sample has some small distortions, its effective mosaic becomes bigger and neutrons in a wider angular range match the Bragg condition. This means that short-range orthorhombic distortions will enhance the Bragg peak intensity and their suppression will reduce the intensity. Hence, we explain the sudden increase of the (2,0,0) Bragg intensity on cooling below $T = 70$ K by the formation of orthorhombic microdomains. This rise reverses on cooling below T_c expected from the competition between orthorhombicity and superconductivity. Analogous measurements in the overdoped sample show much smaller features at or above T_c (Fig. 3b). Consistent with the above explanation, the flat region in the temperature dependence of the TA mode is strongly reduced there as well (Fig. 2e). The fact that $C_{66}(T)$ does not have a feature at 70 K at optimal doping means that orthorhombic microdomains have an effect on elastic properties only at nonzero q probed by

inelastic neutron scattering.

We now discuss behavior below T_c . The most striking feature here is the divergence between small nonzero \mathbf{q} , i.e. results of phonon measurements, and $\mathbf{q} = 0$, i.e. results for C_{66} . Figure 4 shows that phonon softening below T_c becomes more pronounced in the optimally doped sample as \mathbf{q} approaches zero, yet at $\mathbf{q} = 0$ resonant ultrasound [21] and 3-point-bending measurements [19] reveal a pronounced hardening as opposed to softening (square in Fig. 4). The solid and dashed lines in Figure 4 describe the observed momentum dependence (solid line) and extrapolate to the negative value at $\mathbf{q} = 0$ (dashed line), respectively. Hence, there has to be a maximum at a certain wave vector \mathbf{q}_{max} and a zero effect at \mathbf{q}_0 . Obviously, their precise values are not determined in our study. Still we indicate them on the dashed line for discussion. The overdoped sample exhibits the same trend: There is no observable softening below T_c at $h \approx 0.1$ (Fig. 2f), but at $h \approx 0.05$ the softening that starts at 150 K continues below T_c (Fig. 2e). Again this is in contrast to an increase (hardening) of C_{66} in a similarly, i.e. $x = 9.3\%$, doped sample (Fig. 2e) [19].

Discussion

Our results show that the competition between nematic fluctuations and superconductivity is limited to a small range of wavevectors very close to the zone center ($|\mathbf{q}| < 0.04$ r.l.u.). The simplest scenario that explains our data is that $|\mathbf{q}| > 0$ nematic fluctuations intensify on cooling at low temperatures independent of superconductivity, and any features at T_c are due to an indirect effect of superconductivity suppressing orthorhombicity. It is not clear if superconductivity causes some of the enhancement of $|\mathbf{q}| > 0$ nematic fluctuations.

Either way, according to the classic theory of critical fluctuations, the temperature-dependence of the fluctuation spectrum should not abruptly change sign in the vicinity of the ordering wavevector. The observed behavior in the superconducting phase is anomalous and needs to be explained in order to understand the relation between nematicity and superconductivity in Fe-based superconductors. In particular, it needs to be worked out what physics define the wave vector \mathbf{q}_0 , at which the sign change from phonon softening to hardening occurs.

We note that density-functional-perturbation-theory (DFPT) calculations claim that conventional electron-phonon coupling is very weak and unimportant in Fe-based superconductors with regard to the high superconducting transition temperatures [12]. However, it predicts the splitting in energy of certain degenerate phonon modes on going from the high-temperature tetragonal to the low temperature orthorhombic unit cell [28]. Such splitting was recently measured to be much smaller than predicted [29]. These calculations work on the mean-field level, and their quantitative disagreement with experiment reflect the suppression of ordered moment by fluctuations. The phonons that we investigated here are not sensitive to the ordered moment but rather to fluctuations that are not included in DFPT. So, invoking DFPT is of limited utility in explaining our results.

To conclude, we showed that nematic fluctuations at $|\mathbf{q}| > 0.04$ r.l.u. in $\text{Ba}(\text{Fe}_{1-x}\text{Co}_x)_2\text{As}_2$ are enhanced in the tetragonal phase all the way down to the lowest temperatures, and are suppressed by long-range or short-range static nematic order. Their temperature-dependence in the tetragonal non-superconducting phase qualitatively follows the theory of critical fluctuations in that it is similar to that of the fluctuations at the ordering wavevector, $\mathbf{q} = 0$. Below the superconducting transition, however, we observe two qualitatively different regimes: resonant ultrasound [21] and 3-point bending experiments [19] that probe $\mathbf{q} = 0$ show hardening, whereas the phonon measurements that probe $|\mathbf{q}| > 0.04$ r.l.u. show softening. We found that the suppression of the orthorhombic order parameter by superconductivity initiates the onset of softening at T_c in optimally-doped and underdoped samples, but this softening is greater than expected just from the competition between superconductivity and orthorhombicity. In the overdoped sample, which is far from the structural instability, T_c has only a very small measurable effect on the phonons with the softening at $h = 0.04$ continuing the trend that starts

well above T_c (see Fig. 2e). Thus, the phonon softening in the superconducting phase of $\text{Ba}(\text{Fe}_{1-x}\text{Co}_x)_2\text{As}_2$ is a result of an incipient nematic order and superconductivity has only an indirect effect via the suppression of orthorhombic distortions. The surprising momentum dependence of the underlying nematic fluctuations needs to be addressed for a deeper understanding of the interplay of nematicity and superconductivity.

Materials and Methods

The compositions of self-flux grown single crystals of $\text{Ba}(\text{Fe}_{1-x}\text{Co}_x)_2\text{As}_2$ were determined by single-crystal x-ray diffraction. The inelastic neutron scattering experiments were performed on the 4F2 cold triple-axis and on the 1T thermal triple-axis spectrometers at the ORPHEE reactor (Laboratoire Leon Brillouin (LLB), Saclay, France) and on the BT-7 thermal triple-axis spectrometer at NIST center for neutron research (NCNR), Gaithersburg. We investigated two underdoped samples with slightly different doping levels of $x = 4.5\%$ and $x = 4.7\%$, one optimally-doped sample, $x = 6\%$, and an overdoped sample, $x = 9.5\%$. The $x = 4.5\%$ sample was measured at NCNR and the others at LLB. For simplicity, we use the tetragonal notation for wave vectors throughout the text. Wave vectors are given in reciprocal lattice units (r.l.u.) of $(2\pi/a, 2\pi/a, 2\pi/c)$ where a and c are the lattice constants of the tetragonal unit cell.

Acknowledgments

We thank R. Fernandez and J. Schmalian for useful discussions and suggestions. F.W. was supported by the Helmholtz Young Investigator Group under contract VH-NG-840. D.R. was supported by the DOE, Office of Basic Energy Sciences, Office of Science, under Contract No. DE-SC0006939.

D.R. and L.P. conceived the project. T.W. grew the single-crystal samples. M.M. characterized the samples and determined the substitution level. Inelastic neutron scattering measurements at LLB were carried out by F.W., L.P., J.C. and D.R. Similar measurements at NCNR were performed by D.P. F.W., L.P. and D.R. prepared the figures and wrote the manuscript. The authors declare no competing financial interests.

References

- [1] S. A. Kivelson, E. Fradkin, and V. J. Emery, *Nature* **393**, 550 (1998).
- [2] E. Fradkin, S. A. Kivelson, M. J. Lawler, J. P. Eisenstein, and A. P. Mackenzie, *Annual Review of Condensed Matter Physics* **1**, 153 (2010).
- [3] K. Machida, *Physica C: Superconductivity* **158**, 192 (1989).
- [4] J. M. Tranquada, B. J. Sternlieb, J. D. Axe, Y. Nakamura, and S. Uchida, *Nature* **375**, 561 (1995).
- [5] J. M. Tranquada, D. J. Buttrey, V. Sachan, and J. E. Lorenzo, *Physical Review Letters* **73**, 1003 (1994).
- [6] S. A. Kivelson, I. P. Bindloss, E. Fradkin, V. Oganesyan, J. M. Tranquada, A. Kapitulnik, and C. Howald, *Reviews of Modern Physics* **75**, 1201 (2003).
- [7] F. Krüger, S. Kumar, J. Zaanen, and J. Van Den Brink, *Physical Review B* **79**, 054504 (2009).
- [8] W. Lv, J. Wu, and P. Phillips, *Physical Review B* **80**, 224506 (2009).
- [9] C. C. Chen, J. Maciejko, A. P. Sorini, B. Moritz, R. R. P. Singh, and T. P. Devereaux, *Physical Review B* **82**, 100504 (2010).
- [10] S. Nandi *et al.*, *Physical Review Letters* **104**, 057006 (2010).
- [11] G. R. Stewart, *Reviews of Modern Physics* **83**, 1589 (2011).
- [12] L. Boeri, O. V. Dolgov, and A. A. Golubov, *Physical Review Letters* **101**, 026403 (2008).
- [13] Z. Yin, S. Lebegue, M. Han, B. Neal, S. Savrasov, and W. Pickett, *Physical Review Letters* **101**, 047001 (2008).
- [14] I. I. Mazin, M. D. Johannes, L. Boeri, K. Koepernik, and D. J. Singh, *Physical Review B* **78**, 085104 (2008).
- [15] T. Yildirim, *Physica C: Superconductivity* **469**, 425 (2009).
- [16] T. Yildirim, *Physical Review Letters* **102**, 037003 (2009).
- [17] U. Karahasanovic and J. Schmalian, *Physical Review B* **93**, 064520 (2016).
- [18] R. M. Fernandes, A. V. Chubukov, and J. Schmalian, *Nature Physics* **10**, 97 (2014).
- [19] A. E. Böhrer, P. Burger, F. Hardy, T. Wolf, P. Schweiss, R. Fromknecht, M. Reinecker, W. Schranz, and C. Meingast, *Physical Review Letters* **112**, 047001 (2014).
- [20] J.-H. Chu, H.-H. Kuo, J. G. Analytis, and I. R. Fisher, *Science* **337**, 710 (2012).
- [21] M. Yoshizawa *et al.*, *Journal of the Physical Society of Japan* **81**, 024604 (2012).
- [22] J. L. Niedziela, D. Parshall, K. A. Lokshin, A. S. Sefat, A. Alatas, and T. Egami, *Physical Review B* **84**, 224305 (2011).
- [23] D. Parshall, L. Pintschovius, J. L. Niedziela, J. P. Castellan, D. Lamago, R. Mittal, T. Wolf, and D. Reznik, *Physical Review B* **91**, 134426 (2015).
- [24] R. M. Fernandes, S. Maiti, P. Wölfle, and A. V. Chubukov, *Physical Review Letters* **111**, 057001 (2013).
- [25] E.-G. Moon and S. Sachdev, *Physical Review B* **85**, 184511 (2012).
- [26] R. M. Fernandes and A. J. Millis, *Physical Review Letters* **111**, 127001 (2013).
- [27] F. Yang, F. Wang, and D.-H. Lee, *Physical Review B* **88**, 100504 (2013).
- [28] D. Reznik *et al.*, *Physical Review B* **80**, 214534 (2009).
- [29] N. Murai *et al.*, *Physical Review B* **93**, 020301 (2016).

Figures

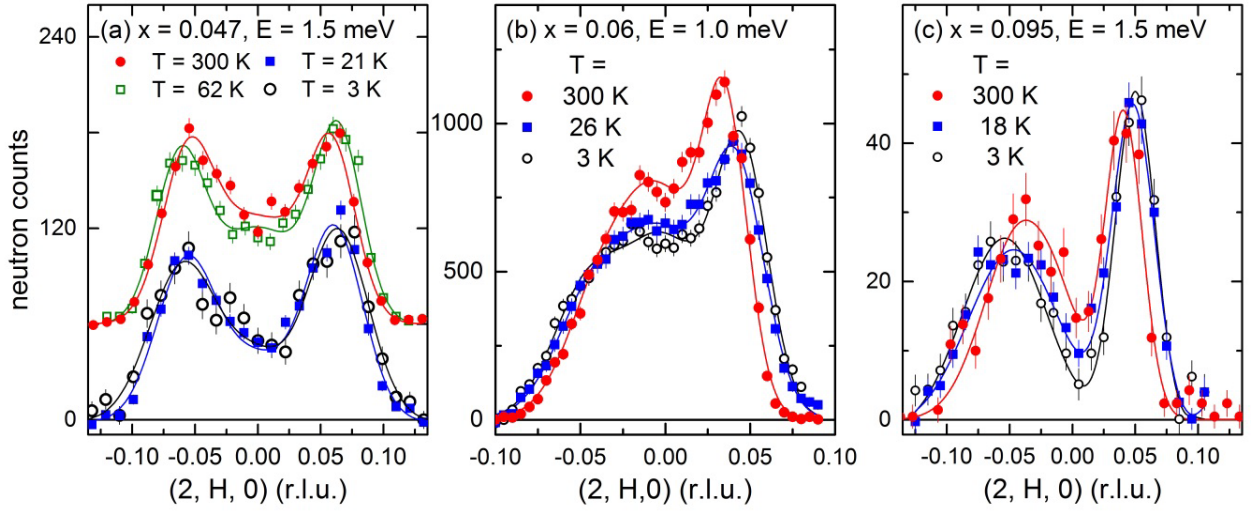


Figure 1: Inelastic neutron scattering in Ba(Fe_{1-x}Co_x)₂As₂. Inelastic neutron scattering data of the transverse acoustic phonon mode in Ba(Fe_{1-x}Co_x)₂As₂ dispersing along [010] direction and polarization parallel to [100]. Measurements were done at fixed neutron energy transfer at (a) $E = 1.5$ meV, (b) $E = 1.0$ meV and (c) $E = 1.5$ meV and $x = 4.7\%$, 6% and 9.5% , respectively. Estimated flat experimental backgrounds were subtracted and intensities corrected for the Bose factor. Inelastic neutron scans are shown for room temperature (dots), just above the respective superconducting transition temperatures T_c (filled squares) and the base temperature (circles). Shift to higher values of H corresponds to a softening. Solid lines are fits to the data as described in the text. In (a) we also show data at $T = 62$ K, which is the structural transition temperature in this underdoped sample. For clarity, we added an offset of 60 neutron counts to the higher temperature data in (a).

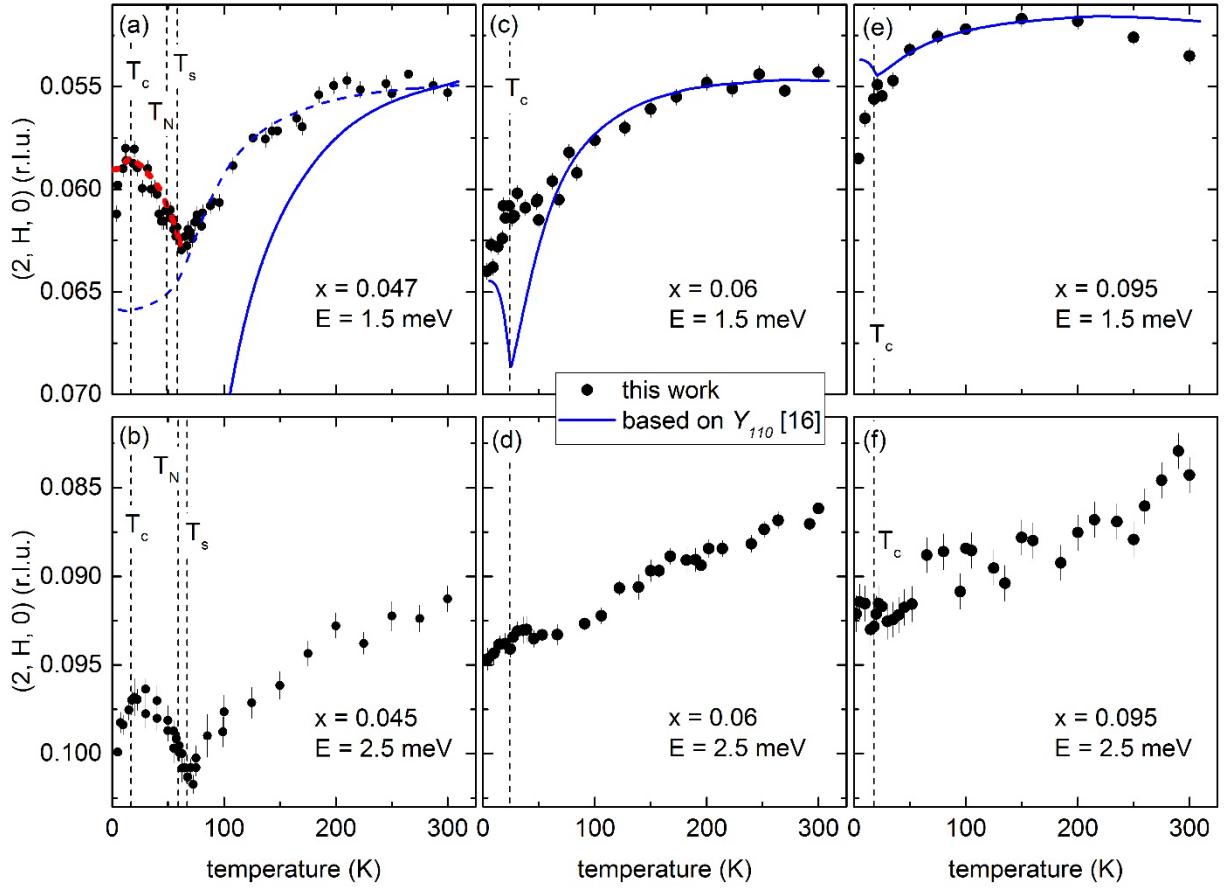


Figure 2: Phonon renormalization in $\text{Ba}(\text{Fe}_{1-x}\text{Co}_x)_2\text{As}_2$. Renormalization of the TA phonon mode in $\text{Ba}(\text{Fe}_{1-x}\text{Co}_x)_2\text{As}_2$ for (a) $x = 4.7\%$, (b) $x = 4.5\%$, (c),(d) $x = 6\%$, (e),(f) $x = 9.5\%$. Constant energy scans (see Fig. 1) were fit to extract the phonon wavevector component H in $\mathbf{Q} = (2, H, 0)$ at constant energies given in the panels. Data in (a) and (b) were taken for two different samples with slightly different transition temperatures indicated by the vertical dashed lines and measured on two different spectrometers (see text). Data shown for identical doping levels were taken on the same sample. For $x \geq 6\%$, samples have only a phase transition to a superconducting state and the respective value of T_c is indicated by the vertical dashed lines. Larger H means a less steep dispersion, i.e. softer phonons. For a more intuitive reading, we plot the H scale upside-down. The short-dashed (red) line in (a) is the orthorhombic splitting measured by neutron diffraction in the sample with $x = 4.7\%$ scaled to the observed phonon hardening in the temperature region $T_c \leq T \leq T_s$. The solid (blue) lines represent the square root of the the Young's modulus $Y_{[110]}$ for (a) $x = 4.3\%$, (c) $x = 6\%$ and (e) $x = 9.3\%$, which is closely related to the C_{66} shear modulus and, hence, the slope of the TA phonon dispersion in the $H \rightarrow 0$ limit. The $Y_{[110]}$ results were taken from Ref. (19) and scaled to fit the minimum values of H observed for the TA mode at $E = 1.5$ meV. The blue dashed line in panel (a) is $(Y_{[110]})^{0.5}$ for $x = 4.3\%$ but the amplitude of the temperature dependence scaled by a factor of 0.25.

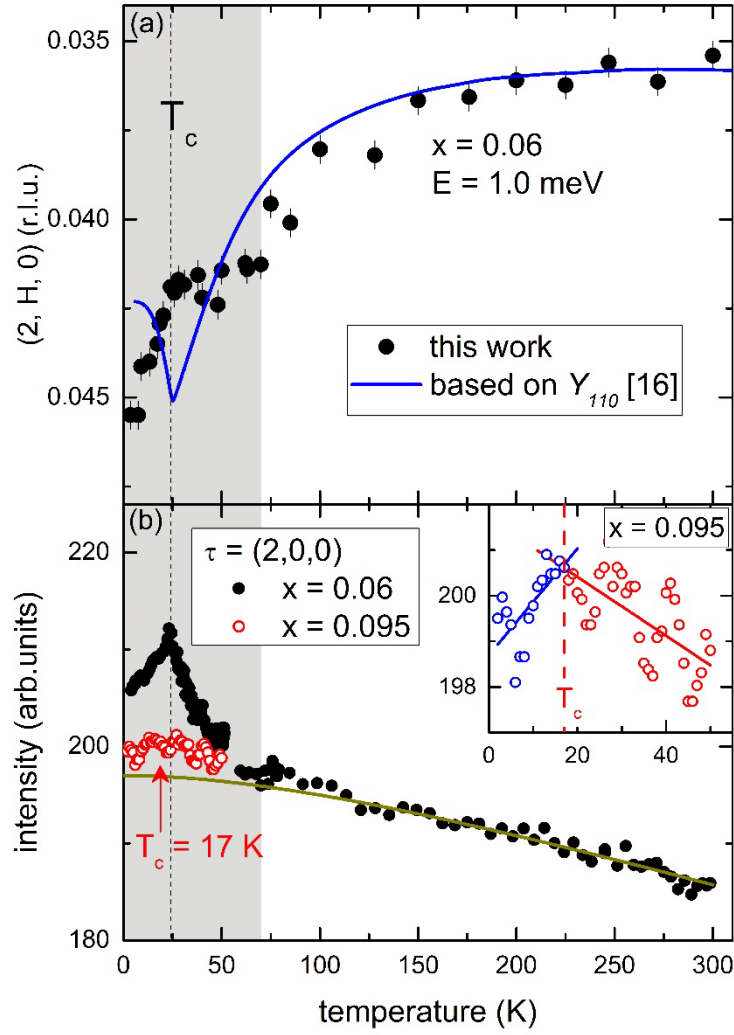


Figure 3: Optimally doped $\text{Ba}(\text{Fe}_{0.94}\text{Co}_{0.06})_2\text{As}_2$. (a) Phonon renormalization in optimally doped $\text{Ba}(\text{Fe}_{1-x}\text{Co}_x)_2\text{As}_2$ at $E = 1.0$ meV. Same symbol/color code as in Fig. 2a-c. (b) Bragg peak intensity of the $(2,0,0)$ reflection as a function of temperature for two different doping levels, i.e. $x = 6\%$ (dots) and 9.5% (circles). The solid line represents the estimated temperature dependence because of the Debye-Waller factor extracted from measurements of the $(6,0,0)$ Bragg reflection. The inset shows the low temperature data for $x = 9.5\%$. Here, linear fits of the low temperature region ($T \leq 16$ K, blue) and higher temperature region ($T \geq 19$ K, red) still show different slopes and, hence, a small T_c effect is still visible. The extracted value of the line crossing at $T = 16.5$ K is in good agreement with T_c measured in magnetization and 3-point-bending for very similar doping levels (19). The grey-shaded areas denote the temperature range for optimally doped $\text{Ba}(\text{Fe}_{0.94}\text{Co}_{0.06})_2\text{As}_2$ featuring orthorhombic micro-domains (see text).

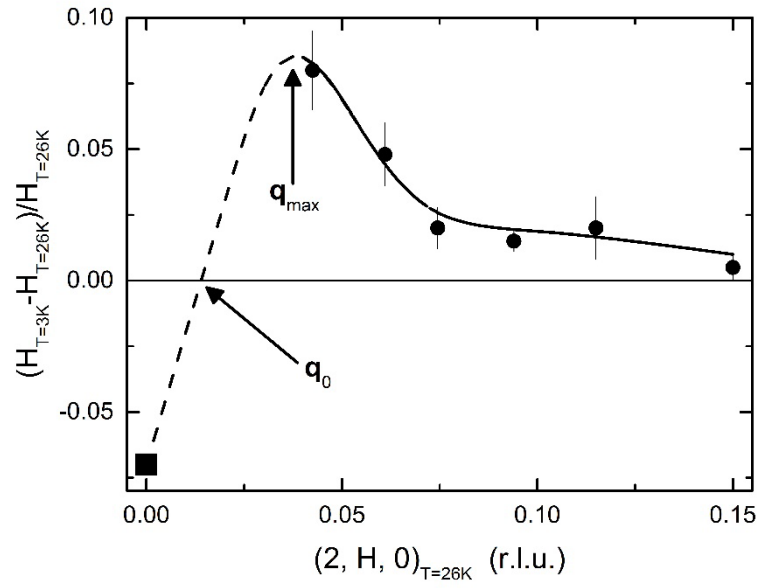


Figure 4: Phonon renormalization below T_c in $\text{Ba}(\text{Fe}_{0.94}\text{Co}_{0.06})_2\text{As}_2$. Relative strength of the phonon softening in the superconducting phase of optimally doped $\text{Ba}(\text{Fe}_{0.94}\text{Co}_{0.06})_2\text{As}_2$ plotted versus the wavevector positions obtained at $T = 26 \text{ K}$ ($\approx T_c$). The solid line is a guide to the eye. The dashed line is a qualitative extension to smaller $|q|$ connecting to the negative value at $H = 0$ (square), reported by RUS (18) and 3-point bending (16) for $x = 6 \%$. See text for the discussion of q_{max} and q_0 .